Ab initio study of hydrogen insertion in ultrathin transition metal doped V films: Structural and electronic properties

A. Lebon and A. Vega*
Laboratoire de Magnétisme de Bretagne, FRE CNRS 3137, Université de Bretagne Occidentale, 6 Avenue Victor Le Gorgeu, 29285 Brest Cedex, France

A. Mokrani
Institut des Matériaux Jean Rouxel, UMR CNRS 6502, Université de Nantes, 2 rue de la Houssinière, B.P. 44322 Nantes, France
(Received 17 November 2009; revised manuscript received 28 January 2010; published 18 March 2010)

We investigate the insertion of hydrogen in ultrathin V films with three monolayers in which we consider a substitutional doping impurity of Ca, Sc, Ti, V, Cr, Mn, and Fe. Calculations are conducted within the density-functional theory, as implemented in the SIESTA code, to analyze the impact of the different doping impurities on the structural shape and, in particular, on the different local environments available for hydrogen insertion, as well as on the electronic structure. The impurities located on the left side of vanadium in the periodic table induce a volume expansion in their neighborhood while elements located on the right side induce a contraction. The embedding energy of the H atom indicates that the impurities at the left act as trapping centers. In general, H prefers tetrahedral interstitial sites in the presence of substitutional impurities at the left of vanadium, whereas octahedral interstitial sites are favored when the substitutional element is at the right. In addition, an increase in the density of states is obtained at the Fermi level when H sits on a tetrahedral site. This H effect can be related with experimental observations of transport properties. Finally, a bonding state is obtained at an energy position that depends on both the substitutional impurity and the symmetry of the interstitial site.

DOI: 10.1103/PhysRevB.81.094110 PACS number(s): 71.20.Be, 75.10.Lp, 75.75.−c

I. INTRODUCTION

Understanding the physics of hydrogen in different geometrical and chemical environments is a relevant issue in material science from both the fundamental and the technological viewpoints. The bonding of hydrogen with its neighborhood can be of different kinds and it can strongly modify the host's structure and electronic properties such as magnetism due to structural relaxation, charge transfer, and hybridization effects. The possibility of modifying the exchange coupling of a magnetic system through hydrogen insertion or the capability of certain host materials to store H are two clear examples of the technological relevance of this topic in the context of spintronics and environmental-clean fuel cell design, respectively.

Concerning the hydrogen storage, many metal-based materials have been studied both experimentally and theoretically, such as the hydrides with alkaline-earth,[1] the borohydrides,[2,3] or the Li-amide-imide compounds.[4] They offer promising weight-storage ratios with hydrogen percentage values as high as 20.8% for the $Mg(BH_4)_2$.[3] All these compounds in crystalline form display a complex sequence of phase transitions, the most interesting structure being only accessible under pressure. Many of them desorb hydrogen at high temperature, like in the highly exothermic chemical reaction of H_2 absorption in Li-amide-imide which leads to a high desorption temperature. Albeit these light-metal hydrides are capable of storing a high density of H, their use is limited by thermodynamical conditions that put in question their suitability for practical applications. In the case of Li-amide-imide host, in order to improve these conditions and performance, substitutional doping with transition metal (TM) atoms is proposed as a mechanism to reduce the reaction enthalpy[4,5] and, therefore, the H desorption temperature.

TM atoms not only play an important role as substitutional impurities in a variety of hosts but they can also form interesting alloys or heterostructures with H storage capability. As far as alloys are concerned, Ti-Cr ones incorporating an homogeneous distribution of V atoms,[6] as well as $LaNi_5$ ones,[7] exhibit promising H storage capability. Other efforts have been devoted to find systems with particular geometry and interfacial properties that allow to control the H absorption. In this context, a recent experimental investigation has shown that Pd-Pt nanoparticles with core-shell structure absorb H atoms particularly at the interface.[8] Remarkably, two elements such as Pd and Pt that display opposite absorption properties in their respective bulks and cluster limits, can form such nanoparticles with interesting storage capability. In general, the geometry and the dimensionality appear as prominent factors when dealing with TM heterostructures in many respects.

Concerning the magnetic properties, superlattices (SLs) of TM/V with TM=Fe, Cr, Mo, have been thoroughly studied both theoretically and experimentally. Specifically, the Fe/V SLs have been investigated to understand the behavior of the interlayer exchange coupling (IEC), e.g., when doping the V spacer with a magnetic element,[9] or through H insertion.[10,11] In the latter case, the H insertion inside the V spacer of Fe_2V_{13} SLs leads to a switch of the IEC coupling from parallel to antiparallel between the Fe layers, in the low H content limit $H/V<0.05$. In the high H content limit $H/V>1$, H loading gives way to a global moment increase.[12] This was explained later on through x-ray measurements at the L_{III} absorption edge of V, that led to no change in moment at V atoms.[13] Consequently, the global increase in magnetic moment upon H loading was attributed essentially to Fe. An

outstanding expansion of the Fe/V superlattice upon H insertion was also observed.[14] Another aspect of the relation between H absorption, lattice distortion, and changes in the magnetic properties of these systems was discussed in a recent theoretical study.[15,16] It was demonstrated that if a magnetic moment as high as $1.1\mu_B$ is artificially induced on V, then the H dissolution is favored.[15] Moreover, it has been clearly stated that the H insertion (necessarily accompanied by a volume expansion) is more favorable when the shear modulus of the material is low.[16] Elements such as Ti, Ca, and Mg are suggested, as they exhibit low shear modulus and low H bond enthalpy. Low shear modulus guarantees a high H absorption whereas low H bond enthalpy guarantees a low temperature for H release.

H loading in TM/V SLs also affects the evolution of the resistivity as a function of the H content, especially the ratio $\frac{\Delta\rho}{\rho}$. For TM=Cr and Mo, the $\frac{\Delta\rho}{\rho}$ was found to increase up to a maximum value for H/V=0.5 to finally decrease for higher H uptake.[17] Fe/V SLs displayed a very different behavior since the resistivity was continuously increasing as H/V increased up to 1. The absence of maximum for the $\frac{\Delta\rho}{\rho}$ ratio in Fe/V was addressed in a theoretical study.[18] It was then concluded that the c/a ratio and the volume change $\Delta V/V$ in the vanadium spacer during hydrogenation were the most important factors governing the change in resistivity. The Cr/V SLs were further investigated by Eriksson *et al.*[17] The c/a ratio and the volume change $\Delta V/V$ are similar in Fe/V and Cr/V SLs, hence the structural argument invoked so far is no longer relevant and some complementary theoretical work is needed to explain this behavior.

In summary, the following conclusions can be drawn on the basis of the experimental and theoretical studies: (i) transition metal substitutional impurities can favor the H absorption-desorption mechanisms of certain host materials. (ii) Transition metal-based heterostructures, particularly TM/V ones, are exciting systems in the context of H absorption and its impact on the electronic properties and structural changes, (iii) the local geometrical and chemical environments can play an important role, (iv) H absorption and H release can be different in different neighborhoods and it should be favored if the shear modulus of the host and the *X*-H bond enthalpy could be reduced.

In a previous work we focused on hydrogenated Fe/V systems belonging to the two limiting dimensionalities of the free-standing clusters and the bulk regime (Fe-V-H trimers and B2 FeV alloys).[19] In the present work we complement this investigation by conducting calculations in the ultrathin film regime and we further study the effect of doping with a variety of substitutional atomic impurities which may affect the H storage properties and the electronic properties. For this purpose, we have built up a system composed of three monolayers of vanadium in which a transition metal doping atom replaces a V one at the central layer. This thin-film configuration belongs to an intermediate dimensionality (between the trimers and the B2 alloys investigated previously). The substitutional impurities preserves the nearest-neighbor atomic coordination of the B2 alloys and, at the same time, finite-size effects typical of free clusters are present due to the surface-vacuum interfaces.

We have chosen to span the fourth row of the Mendeleev table around V, since Ca, Sc, Ti have smaller shear modulus than V, whereas Cr and Fe display a much higher one. All the data concerning the shear modulus, the bond enthalpy, the atomic weight, and the atomic radius are gathered in Table I. These particular elements are chosen because they cover a broad range of shear modulus and atomic radius around those of V in the 3*d* row.

TABLE I. The values of the shear moduli, the H bond enthalpy, and the atomic weight for the investigated elements [source: www.webelements.com and Cordero *et al.* for the atomic radius (Ref. 20)]. No data have been found for the shear modulus of Mn.

Element	Shear modulus (GPa)	*X*-H bond enthalpy (kJ mol^{-1})	Atomic weight (g mol^{-1})	Atomic radius (Å)
Ca	7.6	167.8	40.0	1.76
Sc	28.9	180.0	45.0	1.70
Ti	43.9	204.6	47.9	1.60
V	46.7	208.7	50.9	1.53
Cr	115.3	190.0	52.0	1.39
Mn		234	54.9	1.39(1.61)
Fe	81.8	180.0	55.9	1.32(1.52)

The essential technical details of the calculations carried out in this work are described in Sec. II. In Sec. III we discuss the effects of *X* substitution of a V atom obtained before H loading. Section IV is devoted to the study of the H adsorption and absorption at the different positions close to the substitutional impurity and its relation with the electronic and structural properties. In Sec. V we summarize our main conclusions.

II. THEORY AND COMPUTATIONAL DETAILS

Our calculations have been performed using the *ab initio* density-functional theory (DFT) code SIESTA (Refs. 21–23) which employs linear combination of pseudoatomic orbitals as basis sets. We calculated the exchange and correlation potential with the generalized gradient approximation (GGA) as parameterized by Perdew, Burke, and Ernzerhof.[24] The nonlinear core corrections[25] are included to account for the significant overlap of the core charge with the valence *d* orbitals and to avoid spikes which often appear close to the nucleus when the GGA approximation is used. We replaced the atomic core by a nonlocal norm-conserving Troullier-Martins pseudopotential[26] which was factorized in the Kleinman-Bylander form.[27]

All the data for generating the pseudopotentials is gathered in Table II. The 3*p* semicore states have been taken out from the cores of Ca, Sc, Ti, V, and Cr to achieve a more realistic description of the properties of the system.[30] In the case of V atoms, this has been shown on the one hand to considerably improve the description of the magnetic trends in semi-infinite systems[31,32] and on the other hand it improves the interatomic distance of the dimer.[19]

We also note that the electronic configuration used to generate the Fe pseudopotential corresponds to an excited state (see Table II) because this pseudopotential is known to re-

TABLE II. Valence configuration and cutoff radii (in bohr) for the generation of the Troullier-Martins pseudopotentials used in this work, all within the nonlocal exchange-correlation functional of Perdew-Burke-Erhezenof (Ref. 24). The nonlinear core corrections are included at radius r_{nlcc}.

Atom	Configuration	s	p	d	r_{nlcc}
Ca	[Ne $3s^2$]$3p^6 3d^0 4s^2$	2.80	1.40	1.60	2.45
Sc[a]	[Ne $3s^2$]$3p^6 3d^1 4s^2$	2.57	1.08	1.37	
Ti	[Ne $3s^2$]$3p^6 3d^2 4s^2$	2.50	2.20	2.20	1.10
V[b]	[Ne $3s^2$]$3p^6 3d^3 4s^2$	2.50	2.17	0.90	1.20
Cr	[Ne $3s^2$]$3p^6 3d^5 4s^1$	2.33	1.30	1.49	0.80
Mn[c]	[Ar]$3d^5 4s^2 4p^0$	1.98	2.18	1.88	
Fe[b]	[Ar]$3d^7 4s^1 4p^0$	2.00	2.00	2.00	

[a]Reference 28.
[b]Reference 19.
[c]Reference 29.

produce the correct spin state of Fe dimers.[33] We have tested that these pseudopotentials accurately reproduced the eigenvalues of different excited states of the respective isolated atoms.

Concerning the basis sets, we have described the valence states using double ζ polarized pseudoatomic orbitals, further referred to as DZP. The basis set of Fe and Mn included two orbitals having different radial form to describe both the 4*s* and the 3*d* shells, being the 4*s* polarized to include a single orbital for the empty *p* shell. In the case of Ca, Sc, Ti, V, and Cr, we considered two orbitals having different radial form to describe the 3*p*, 4*s*, and 3*d* valence states, being the 4*s* single polarized. A 350 Ry energy cutoff defines the real-space grid to compute the exchange and correlation potential and to perform the real-space integrals that yield the Hamiltonian and overlap matrix elements. We also smoothed the Fermi distribution function that enters in the calculation of the density matrix with an electronic temperature of 300 K. The same theoretical approach was used in our recent study of free-standing Fe-V-H trimers and B2 FeV alloys.[19]

A (001) bcc ultrathin film of three vanadium monolayers, called TL^{*V}, has been modeled using a supercell with 48 nonequivalent atoms (49 when the H atom is inserted) and periodic boundary conditions, inserting enough vacuum space along the (001) direction to avoid interaction between the surfaces of neighboring cells. The estimation of the required vacuum space to separate the surfaces of the V films of neighboring cells ≈ 15 Å is done in terms of the length of the basis functions which are strictly localized in SIESTA. We used a $8\times8\times1$ Monkhorst-Pack *k* grid in the reciprocal space. Using a conjugate gradient method, the atomic and electronic degrees of freedom of the films, with or without H, were allowed to relax simultaneously and self-consistently until interatomic forces were smaller than 0.01 eV/Å. The forces on ions were computed using a variant of the Hellmann-Feynman theorem that includes Pulay-type corrections to take into account the fact that the basis sets are not complete and move with the atoms.[21] Both paramagnetic and spin-polarized calculation were carried out.

For the calculation of both the substitution energies in the TL^{*X} systems and the H absorption energies at the different

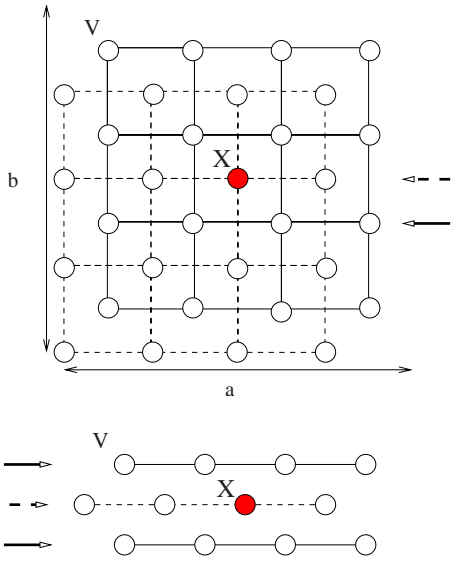

FIG. 1. (Color online) The upper plot shows the top view of the unit cell of our TL^{*X} systems. White balls are V atoms, whereas the red ball is the substitutionnal impurity *X* (*X*=V, Ca, Sc, Ti, Cr, Mn, and Fe). The horizontal and vertical double arrows, *a* and *b*, define the cell parameters for the simulations. The lower plot shows a lateral view of the same systems.

positions, we have considered the ghost atom method to correct the basis set superposition error (BSSE) that arises due to the different dimension of the Hilbert spaces associated to the initial and final systems whose energy difference is computed, which otherwise would imply different degrees of freedom in the variational determination of the energy of each system. The ghost atom means additional basis wave functions centered at the atomic position where it is located but without any atomic potential. The use of ghost atoms has been shown to be very efficient for correcting the BSSE in other systems such as, for instance, benzene adsorbed on carbon nanotubes[34] or pentacene physisorbed on gold (001).[35] To calculate the energy required to create a vacancy in the three monolayers of V atoms, we calculate the difference between the total energy of the thin film and the sum of: (i) the total energies of the isolated V atom represented by the same system built of ghost atoms except the real V one and (ii) the three monolayers with a ghost atom located in the vacancy site.

III. EFFECT OF DOPING ON THE INTERSTITIAL SITES

The unit cell used for modeling the TL^{*X} system is illustrated in Fig. 1. It corresponds to a low impurity concentration of about 2%. In Fig. 2 we show the different sites for H inserted or anchored to the surface. H can occupy different tetrahedral (T) or octahedral (O) positions. The H atom has been inserted in the neighborhood of the doping impurity.

First of all we substitutionally inserted the doping atom inside the three monolayers to form the TL^{*X} system and fully relaxed it. The substitution impurity preserves the tetragonal symmetry of the system.

The substitutional energy of one vanadium atom by the *X* impurity $\Delta E_{X\rightarrow V}$ is calculated as the sum of the substitutional

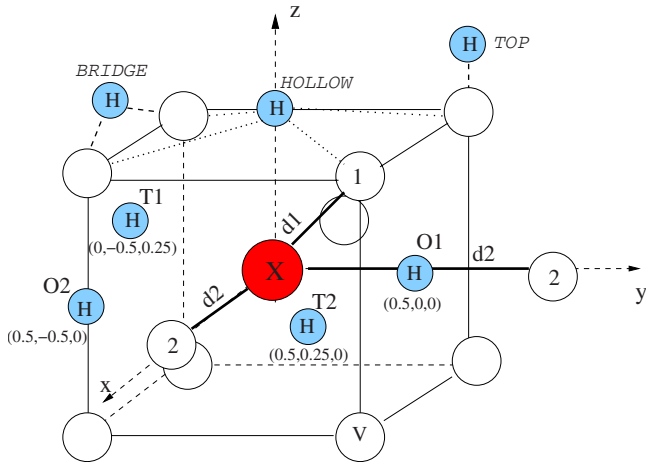

FIG. 2. (Color online) The sites with different symmetry available for H insertion in TL^{*X} (upper plot). The color convention is the same as in Fig. 1 for V and X, and the H atom appears as a light blue ball. The surface adsorption sites are called TOP, BRIDGE, and HOLLOW. The reduced coordinates of the tetrahedral (T1, T2) and octahedral (O1, O2) sites are given in parenthesis. 1 and 2 labels in V balls designate a first and second neighbor of impurity X that pertain to the polyhedron of coordination of H.

energy of one vanadium by a vacancy $\Delta E_{vac\to V}$ and the substitutional energy of this vacancy by the X impurity $\Delta E_{X\to vac}$,

$$\Delta E_{vac\to V} = [E(TL^{*0}) + E(V)] - E(TL^{*V}) \quad (1)$$

$$\Delta E_{X\to vac} = E(TL^{*X}) - [E(TL^{*0}) + E(X)]. \quad (2)$$

$E(TL^{*V})$ is the energy of the pure V film, $E(TL^{*0})$ and $E(TL^{*X})$ are the energies of the film system in which a V central atom is substituted by vacancy and X impurity, respectively. These energies are calculated using BSSE correction and full structure relaxation around the impurity.

The substitutional energy

$$\Delta E_{X\to V} = \Delta E_{vac\to V} + \Delta E_{X\to vac} \quad (3)$$

normalized to one unit cell, is listed in the last line of Table III for the different substitutional atoms. The pure vanadium film is nonmagnetic and only when doping it with Fe, it becomes magnetic, with $1\mu_B$ in the Fe impurity and $0.03\mu_B$ in the nearest V neighbors (antiparallel coupling between Fe and V). This solution is about 0.5 meV/atom more stable than the nonmagnetic one. No significant structural change is observed. For a low impurity concentration, these results are consistent with recent Green's-function calculations in the coherent-potential approximation,[9] in which V layers doped with TM magnetic impurities (TM=Fe,Co,Cr,Ni) were paramagnetic for impurity content below 10%. Furthermore, structural differences are minimal between both solutions, as we will see later. Although in all cases the process is endothermic, the energy cost for the Ti substitutional doping is an order of magnitude lower than that of all the other TM considered (two orders of magnitude lower than that of Ca). Table III also reports the distances between the impurity and its different V neighbors up to the fourth one, d_1, d_2, d_3, and d_4.

TABLE III. Distances between the impurity X and its first, second, third, and fourth V neighbors (d_1, d_2, d_3, and d_4). All distances are given in angstrom. Results in parenthesis are for the paramagnetic solution when X=Fe. The energy of substitution is added in the last line and is given in electron volt.

	Ca	Sc	Ti	V	Cr	Mn	Fe
d_1	2.84	2.75	2.62	2.53	2.49	2.47	2.50(2.50)
d_2	3.04	3.02	3.01	3.01	2.98	2.95	2.96(2.95)
d_3	4.33	4.28	4.26	4.25	4.24	4.22	4.23(4.22)
d_4	5.00	4.99	4.97	4.95	4.93	4.91	4.90(4.90)
$\Delta E_{X\to V}$	6.048	2.116	0.048	0.000	1.565	1.171	0.511

Doping with Ca, Sc, or Ti increases the neighbor distances, particularly the nearest-neighbors' ones (see Table III). On the contrary, doping with Cr, Mn, or Fe decreases the neighbor distances. These results correlate with the differences in the respective atomic radius (Table I). We note that Ca (the only element here not belonging to the $3d$ series) generates important local distortions, both in the octahedral and tetrahedral environments. For instance, the difference d_2-d_1 reported in Table III is minimum for Ca (0.20 Å) whereas the maximum value is obtained for Cr (0.49 Å). This explains why the Ca substitution is so endothermic; it costs a considerable energy to displace the vanadium atoms in the surrounding of the substitutional Ca atom. On the other side, we note that doping with Cr and Fe, two elements that crystallize in the bcc structure like V, leads to small and comparable structural changes. The case of the X=Sc appears as intermediate between Ca and the other TM elements.

As regards the H insertion in the TL^{*X} system (this will be discussed in the next section) it is worth to quantify the changes in the local volume Ω(H) available for the H insertion in the different interstitial sites upon X doping. In Fig. 2 we illustrate the different positions for H insertion. Two tetrahedral and two octahedral insertion sites exist in the TL^{*X} system, named T1, T2, O1, and O2. Possible interstitial sites at different distances from the impurity are shown in Fig. 3.

The variation in Ω(H) induced by the substitutional impurity is plotted in Fig. 4. We have found that changes in the local volume are strictly localized close to the doping atom for the O1 and T1 sites, independently of the doping element, whereas they are more delocalized for the O2 and T2 sites, with even marked oscillations in T2. An increase in Ω(H) is obtained after substitutional doping with Ca, Sc, and Ti, whereas substitution with Cr, Mn, or Fe leads to a decrease in Ω(H). Therefore, the decrease in electron density when substitutionally doping with Ca, Sc, and Ti (at the left of V in the periodic table) correlates with an increase in the volume available for H insertion, whereas the opposite occurs with an increase in the electron density when substitutionally doping with Cr, Mn, and Fe (at the right of V in the periodic table).

The variation in Ω(H) is less than 1% for H-X distances larger than 5.0 Å when X=Ti, Cr, Mn, and Fe. We note that this critical distance fits the three monolayers vanadium region depleted of H, experimentally observed[36] and theoreti-

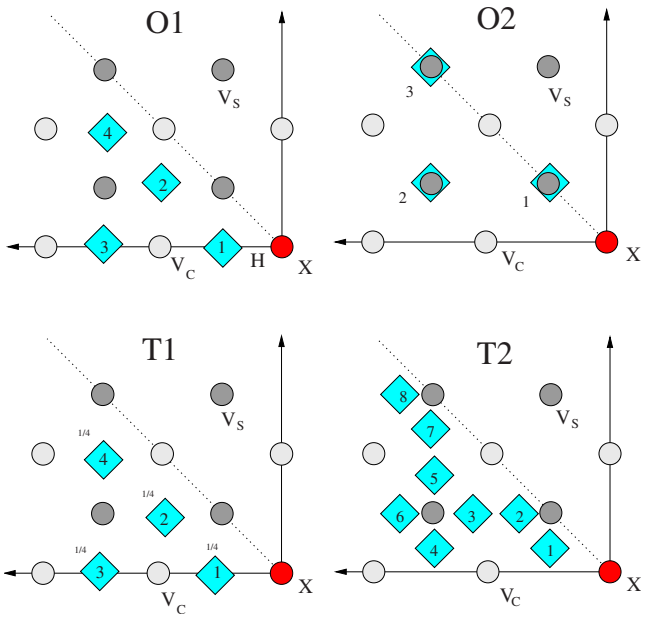

FIG. 3. (Color online) A top view of an eighth of the unit cell of TL^{*X} is shown for symmetry reasons. O1, O2, T1, T2 correspond to different octahedral and tetrahedral sites of the symmetry depicted in Fig. 2. The X atom appears as a red ball, the interstitial sites are depicted as light blue diamond. The light gray balls are V atoms at the central layer and the dark gray ones are V atoms at the surface layer. The smaller the number within the diamond, the smaller the distance to the impurity atom X. The symbol 1/4 indicates that the T1 interstitial sites are located $1/4c$ above the central layer.

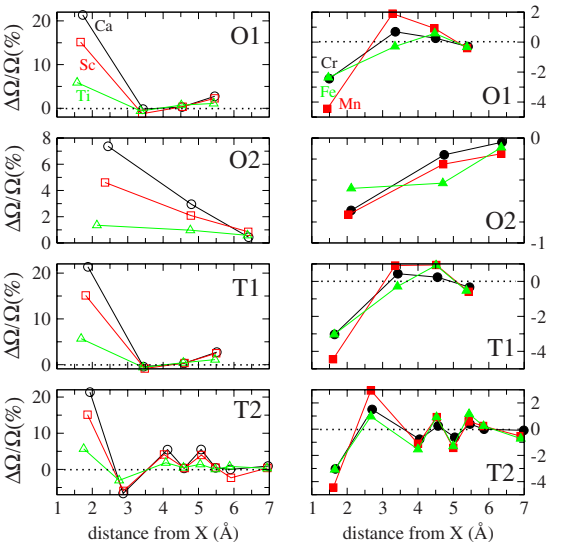

FIG. 4. (Color online) Change of the volume available for H insertion after substitutional doping of the V film with impurity. A positive (negative) variation means a volume increase (decrease). The left panels correspond to the doping with X=Ca, Sc, and Ti. The open black circle is for Ca, the open red square for Sc, and the open green triangle for Ti. The right panels correspond to the doping with X=Cr, Mn, and Fe. Full black circle is for Cr, full red square for Mn, and finally full green triangle for iron. The dotted line at 0 in all panels is the reference of the different tetrahedral and octahedral volumes within the undoped TL^{*V} system, that is, with no volume change.

cally obtained[16] in Fe/V and Cr/V multilayers. Although the local environments are different in the interfacial Fe/V and Cr/V films and in our diluted doped system, the trends are consistent. We also obtain that the distortion induced by Ti is opposite to the one induced by Cr doping.

We have calculated the densities of states projected on the different substitutional impurities, which show that for the 3d transition metal elements, the 3d character of the bonding prevails. For X=Ca, however, the 4s state has a larger contribution at the Fermi energy. This outer delocalized 4s shell of Ca might have an impact on the substantial changes obtained in the V film after doping.

In summary, from the structural point of view, the main contribution of doping is to increase or decrease the available volume for H insertion especially in the immediate vicinity of the X impurity. This volume is not uniform along the whole system and might be tuned by an appropriate choice of the doping elements.

IV. H-LOADED SYSTEMS

The energy cost of H insertion or adsorption in a given position within the TL^{*X} films is calculated using the following expression:

$$\Delta E_{\mathrm{H}\rightarrow} = E(TL^{*X} + \mathrm{H}) - [E(TL^{*X}) + E(\mathrm{H})], \qquad (4)$$

where $E(TL^{*X}+\mathrm{H})$ stands for the energy of the relaxed three monolayers (doped or undoped) loaded with the H atom. On a surface, H can either occupy TOP, BRIDGE, or HOLLOW sites. In the volume, H is on O1, O2, T1, or T2 sites (Fig. 2). As indicated previously, $E(TL^{*X})$ is the energy of the H free V film doped with Ca, Sc, Ti, V, Cr, Mn, or Fe. E(H) is the energy of the isolated H atom.

A. H loading in the undoped V film

Let us analyze first the H insertion in the undoped V film. In Table IV we list the values obtained for the different energy costs of H insertion or adsorption $\Delta E_{\mathrm{H}\rightarrow}$, changes in the

TABLE IV. Results are given for the H insertion energy in the different sites of the undoped TL^{*V} system; the in-plane distortions (Δa,Δb) the charge transfer of the H atom and the distance of H with its first and second V neighbors (in angstrom) when this distance does not exceed 3 Å.

H position	$\Delta E_{\mathrm{H}\rightarrow}$ (eV)	Δa (pm)	Δb (pm)	δQ_{H} (e)	d_{HV} (Å)
TOP	−2.104	−5	−5	+0.30	1.773
BRIDGE	−2.704	−5	−2	+0.20	1.876
HOLLOW	−2.727	0	0	+0.10	1.943, 2.193
O1	−1.394	+1	+8	−0.49	1.700, 2.026
O2	−1.489	−13	−13	−0.20	1.776, 2.077
T1	Unstable				
T2	−1.578	0	0	−0.35	1.743, 1.774

in-plane cell parameters (Δa and Δb), resulting charge transfer in H, and distance of H with its nearest V neighbors. For the surface adsorption, the energetically preferred position is the hollow site which leads to a negligible structural change together with a very favorable $\Delta E_{H\rightarrow}$. All surface sites are more stable than internal ones. Among the internal ones, the most favorable site for H insertion is the tetrahedral position T2, for which we obtain the smallest structural reconstruction. Both internal T2 and surface HOLLOW sites present a bonding of H with a pair of vanadium atoms that is reminiscent of the stable configuration of the V+V+H trimer, found in our previous work,[19] in which H forms an isosceles triangle with the V-V dimer and sits on the summit of the triangle. The results for T2 site are in agreement with bulk data for vanadium bcc.[19] Inserting H in the octahedral sites produce larger structural distortions, as illustrated by the variation in Δa and Δb (Fig. 1). Therefore, it costs more energy to insert H in an octahedral site than in a tetrahedral site, whereas the insertion in T1 results unstable and the H atom comes out of the system as if no diffusion barriers to the surface existed at this position.

H has a trend to capture charge at the surface where it hybridizes with the dangling bonds of the vanadium atoms. On the contrary, when inserted in the V matrix, H donates a noticeable amount of charge to its vanadium neighbors whatever the insertion site. This charge transfer in the ultrathin film configuration exceeds the charge transfer found by Duda *et al.*[37] in their combined x-ray absorption spectroscopy (XAS) and full-potential linear muffin-tin orbital calculations of the Fe/V SLs. These authors estimated a charge transfer from H to the V matrix of about $0.25e^{-}$.

In Fig. 5 we plot the local 3*d*-projected density of states of V and the 1*s*-projected density of state of H in the H-free and H-loaded V films of three monolayers. The insertion of H gives rise to a bonding state around ≈ -8.0 eV below the Fermi energy. This peak is ≈ 5.0 eV below the bottom of the 3*d* bands. This peak is at -7.98 eV for the O1 site and it is found at -7.73 eV for the T2 site. This difference of energy partially explains the broadening of the peak observed through XAS in H-loaded V systems. H atoms first sit in tetrahedral sites and then in octahedral sites. In the experimental work of Duda *et al.*,[37] the pressure used leads to a ratio of H/V of 0.5 that compels the H atom to share octahedral an tetrahedral sites.[38] Thus, the XAS data exhibits a broad peak that may result from the average contributions from the two kind of insertion sites. The energy difference between the location of the peak for the T2 and O1 H insertion sites (0.25 eV) should be measurable with photoelectron spectroscopy techniques and the T2 to O1 site transition should appear in the spectra. A low-energy shoulder of the original H 1*s* peak should emerge and progressively constitute the main contribution.

The densities of states in Fig. 5 also show that H insertion in the O1 site do not appreciably modify the V states, whereas if inserted in T2 and O2 sites, it increases the number of 3*d* states of its nearest V neighbors at the Fermi level. This is due to a shift of the main peak of this local density of states toward lower energies, which in turn reflects the gain of electronic charge in the surface V atoms at the expense of H. The increase in the density of states at the Fermi level for

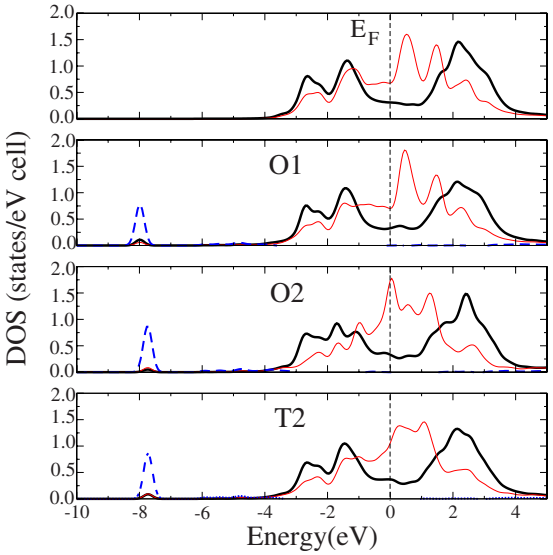

FIG. 5. (Color online) Density of states projected on the 3*d* states of V and on the 1*s* state of H in the H-free (upper plot) and H-loaded (lower plots for different insertion sites) undoped three monolayers of V atoms, TL^{*V}. The lower the plot, the lower the energy cost of H insertion. The thick black lines correspond to the 3*d* states of the central V atom, the thin red lines correspond to 3*d* states of the first V neighbor of H (located at the surface), and the dashed blue lines correspond to the 1*s* state of H.

the T2 and O2 sites suggests a possible magnetic instability, following the Stoner criterion.

Coming back to Table IV, insertion in T1 sites is unstable and insertion in O2 sites is characterized by a strong contraction of the in-plane simulation cell and an expansion in the out-of-plane direction. This is perhaps the reason why albeit H insertion in O2 sites were computed for all TL^{*X} systems, it failed to converge. Consequently in which follows, devoted to discussing H insertion in the doped TL^{*X} systems, we will focus on the insertion sites O1 and T2.

B. H loading in the doped V film

Let us analyze now the H insertion in the doped TL^{*X} film. Figure 6 shows the data obtained for the H insertion in the O1 or T2 sites closest to the doping atom in the different TL^{*X} films. In Fig. 6(a), the computed insertion energies $\Delta E_{H\rightarrow}$ are displayed for both T2 and O1 sites. The T2 site is the most favorable insertion site for all impurities except Fe. In the case of Mn, T2 could not be stabilized. For X=Ca, Sc, and Ti, the insertion energies in the T2 interstitial site result smaller than the corresponding ones in the pure V thin film. Thus, atoms located on the left side of V in the periodic table exhibit a trend to trap an H atom in their close vicinity. If we disregard X=Fe, atoms at the right of V, such as X=Cr and Mn, seem to repel the H atom. Hence, there is a correlation between the volume expansion created by X=Ca, Sc, and Ti (as illustrated in Fig. 4) and their ability to act as trapping centers for H. On the contrary, for X=Mn or Cr, a contraction of the volume in the neighborhood of the impurity correlates with the less favorable $\Delta E_{H\rightarrow}$. As far as X=Fe is concerned, the O1 site has a very low insertion energy that

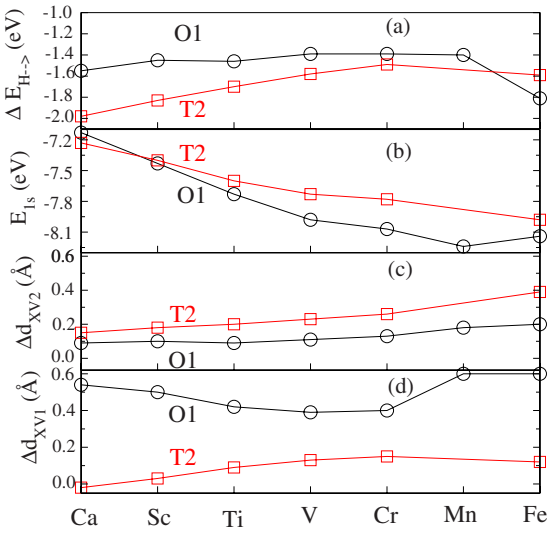

FIG. 6. (Color online) For each doping impurity X and H insertion in O1 and T2 sites we plot: (a) the calculated insertion energy $\Delta E_{H\rightarrow}$, (b) the energy of the bonding state E_{1s} discussed in the text, and in (c) and (d) the variation in the distance between the X impurity and its first and second V neighbors in the doped trilayer of vanadium, loaded with H (TL^{*X}+H).

amounts to $\Delta E_{H\rightarrow}=-1.81$ eV. The structural arguments used with X=Cr and Mn are not valid with X=Fe, and other explanations are to be found. It is worth to mention a recent theoretical work by Dziekan *et al.*,[15] who followed the evolution of the H dissolution energy in the V layers of a Fe/V SL system. By applying a uniform magnetic moment to the V layers, they observed an increase in the dissolution energy of H. In the present case, magnetism could not be invoked to explain the higher stability of the O1 interstitial site. Indeed, the O1 site is favored for both the paramagnetic and the magnetic solutions, this latter solution showing a low-spin state for Fe, with a moment of $1\mu_B$. Moreover, for the B2 alloy system loaded with a H atom, the equivalent position to O1 corresponds to the ground-state configuration in which the Fe moment amounts to $2.2\mu_B$.[19] The H+Fe+V trimers[19] have an environment that may help to understand the higher stability of the O1 site. In fact, as evidenced in Fig. 2 of Ref. 19, H prefers the vicinity of V instead the one of Fe. In a O1 insertion site, H encounters 5 V neighbors and 1 Fe neighbor, thus increasing its number of V neighbors as compared with the T2 site.

The shift of the energy of the bonding state, E_{1s}, is displayed in Fig. 6(b). This bonding energy shifts toward higher energies when the 3d band of the doping element empties. Thus, for X=Ca and Sc, the computed E_{1s} is lower than for X=Mn or Fe. Indeed the electronic configurations of Ca [Ar]$4s^2 3d^0$ and Sc [Ar]$4s^2 3d^1$ have no 3d electrons or just one, respectively. The H 1s-X 3d character of the bonding state is therefore reflected in the position of E_{1s} for the different doping impurities. Consequently it should be possible to identify, using photoelectron spectroscopy, the regions of a doped V system that are rich in a certain impurity close to which the H atoms were located. The projected densities of states are plotted in Figs. 7–9 for X=Ti, Cr, and Fe, respectively. The most striking feature is the appearance of this bonding state.

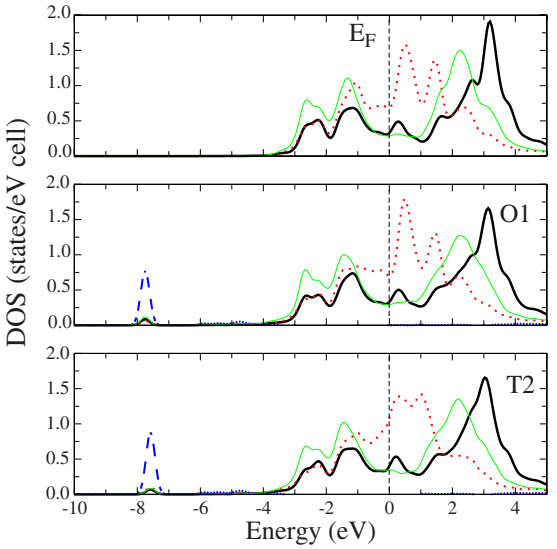

FIG. 7. (Color online) Projected density of states of the TL^{*Ti} system with H inserted within the film, the lower the panel the lower the energy. The thick black line is for the Ti 3d states, the dotted red line corresponds to the V 3d states of the Ti first neighbor, and the thin green lines to the V 3d states of the Ti second neighbor. H 1s state are shown with a dashed blue line.

The behavior of the density of states at the Fermi level, $D(E_F)$, for V and the impurity atom deserves some comments. In fact, for X=Cr and Ti, $D(E_F)$ increases for the nearest V neighbors of X (V at the surface) when H is inserted in the stable T2 site. For X=Fe, $D(E_F)$ also increases for the T2 site although, as mentioned earlier, H prefers inserting in a O1 site, for which $D(E_F)$ keeps constant. Besides, contrary to what happens for X=Ti or Cr, a peak at ≈ -3.0 eV of the density of states projected on the 3d states of Fe, is redistributed after H loading in both T2 and O1

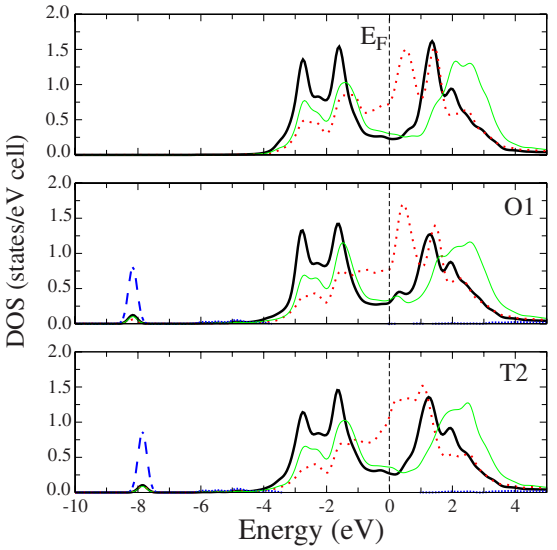

FIG. 8. (Color online) Projected density of states of the TL^{*Cr} system with H inserted within the film, the lower the panel the lower the energy. Here X=Cr. The color convention is the same as Fig. 7, the thick black lines being reserved for the 3d states of Cr.

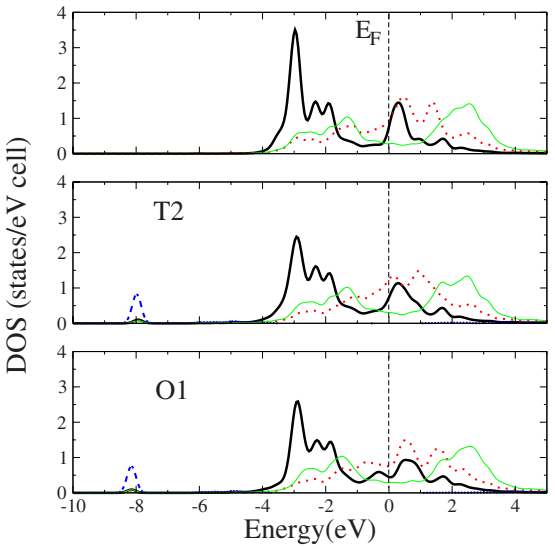

FIG. 9. (Color online) Projected density of states of the TL^{*Fe} system with H inserted within the film, the lower the panel the lower the energy. Here X=Fe. The color convention is the same as Fig. 7, the thick black lines being reserved for the 3d states of Fe.

sites. Two elements such as Fe and Cr that induce a comparable deformation of the cell (see Table III and Fig. 4) favor different interstitial sites, namely, T2 for X=Cr and O1 for X=Fe. This remark is relevant in the context of transport properties reported for the Fe/V and Cr/V SLs systems. Two opposite behaviors for the variation in the resistivity $\frac{\Delta\rho}{\rho}$ were observed as the content of H within the V layer increased up to $H/V \approx 1$. The Fe/V SLs exhibit a monotonic increase of the $\frac{\Delta\rho}{\rho}$ ratio, whereas the Cr/V SLs reach a maximum of $\frac{\Delta\rho}{\rho}$ for $H/V \approx 0.5$ and latter on decreases substantially.[17] In the Ohmic regime, the conductivity is a linear function of the density of states at the Fermi level.[18] In the limit $H/V \approx 1$, the H atoms that enter in the V layers suffer the repulsion by the already inserted H atoms. Thus, the inserted atom in the high concentration limit should sit in the depleted zone and strongly interact with the interface. In view of the present results, it is likely that getting closer to the V/Cr and V/Fe interface, the inserted H atoms modify the transport properties through the variation in the $D(E_F)$. An increase in $D(E_F)$ for the stable T2 site in the TL^{*Cr}+H system should correlate with an increase in the conductivity while the no change in $D(E_F)$ for the stable O1 site in the TL^{*Fe}+H system should correlate with no change in the conductivity as compared with the H-free TL^{*Fe} system.

Finally, in Figs. 6(c) and 6(d) we plot the change in the distances between the X-doping atom and a first and a second V neighbor, referred to as d_1 and d_2, respectively. Those V atoms form part of the polyhedron of coordination of H in the tetrahedral or octahedral sites. They are labeled as 1 and 2 in Fig. 2, respectively. It is obvious from these two panels that H insertion in a T2 or O1 interstitial site locally increases d_1 and d_2. Weaker increase is obtained for the elements located at the left side of the V atom in the periodic table, at least for the stable T2 insertion site, whereas for X=Cr, Mn, and Fe stronger variation is found whatever the insertion site. For X=Ca, Sc, and Ti, the original expansion due to X substitution seems to diminish the expansion generated by H insertion, especially for the T2 insertion site which is the most stable one. On the contrary, a substitution of X=Cr, Mn, and Fe contracts locally the cell. The H insertion in T2 and O1 sites thus leads to a larger expansion, as quantified by the variation in the distances d_1 and d_2. The process implies a volume expansion for the coordination polyhedron of H and gives way to an increased energy cost according to elastic considerations, as invoked in the work of Meded and Mirbt.[16]

Gathering all previous results, it is possible to infer which substitutional element is better suited to improve the H storage capability of V films. Elements located at the left side of V in the periodic table offer space in their neighborhood as they do expand locally the cell and lead to smaller energies of H insertion. In this respect, X=Ca, Sc, and Ti seem promising doping elements for substitution. However, the high substitution energy computed for X=Ca put in question the use of this element at high impurity concentrations. In addition, substitution of V by X=Ca, Sc, Ti decreases the weight of the system and, accordingly, increases the H weight ratio. Concerning Cr, Mn, and Fe as impurity, they seem to prevent hydrogen to sit in their vicinity on the basis of structural considerations (local volume contraction). This structural trend is confirmed in the case of Cr and Mn by the computed values of the insertion energy and the energy of the bonding state. For X=Fe, this remark must be contrasted since the insertion energy is small in the O1 site and compares to the value of H insertion in T2 site when X=Sc.

V. CONCLUSIONS

We investigate the insertion of hydrogen in ultrathin V films with three monolayers in which a substitutional doping impurity X=Ca, Sc, Ti, V, Cr, Mn, or Fe is introduced. We use the DFT SIESTA code to analyze the impact of the different doping impurities on the structural shape and different local environments available for the hydrogen insertion, as well as on the electronic structure. The main results are summarized as follows: (i) doping with Ca, Sc, or Ti increases the distances between the impurity and its V neighbors, particularly the nearest neighbors. On the contrary, doping with Cr, Mn, or Fe decreases the neighbor distances. These results are consistent with the differences in the respective atomic radius. As a consequence, an increase in the local volume available for H insertion, Ω(H), is obtained after substitutional doping with Ca, Sc, and Ti, whereas substitution with Cr, Mn, or Fe leads to a decrease in Ω(H). Therefore, the main contribution of doping is to increase or decrease the available volume for H insertion especially in the immediate vicinity of the impurity. This volume is not uniform along the whole system and might be tuned by the appropriate choice of the doping elements.

(ii) Ω(H) is no more affected for distances H-X larger than roughly 5.0 Å when X=Ti, Cr, Mn, and Fe. We note that this critical distance fits the three monolayers vanadium region depleted of H experimentally observed[36] and theoretically obtained[16] in the Fe/V and Cr/V multilayers.

(iii) The insertion of H in the pure V thin film gives rise to a bonding state, E_{1s}, around ≈ -8.0 eV. The energy differ-

ence between the location of this peak for the tetrahedral (T2) and octahedral (O1) insertion sites (0.25 eV) should be measurable with photoelectron spectroscopy, and the T2 to O1 site transition, experimentally observed, should appear in the spectra. A low-energy shoulder of the original H 1*s* peak should emerge first and progressively constitute the main contribution.

(iv) The T2 site is the most favorable insertion site for all substitutional impurities, except Fe and Mn. The insertion energies in the T2 site result smaller than the corresponding ones for the V atom. Thus, atoms located on the left side of V in the periodic table, i.e., X=Ca, Sc, Ti, exhibit a trend to catch an H atom in their close vicinity, that is, they are trapping centers.

(v) The shift of the energy of the bonding state, E_{1s}, increases with decreasing the *d*-band filling of the doping impurity. Consequently it should be possible to identify, using photoelectron spectroscopy, the regions of a doped V system that are rich in a certain impurity close to which the H atoms were located.

(vi) Different behavior of the density of states at the Fermi level, $D(E_F)$, is obtained for the tetrahedral and the octahedral insertion sites. H insertion in a the octahedral site leads to no change in $D(E_F)$, whereas an increase in $D(E_F)$ is obtained upon H insertion in the tetrahedral site. This can be relevant in the context of recent experiments of transport properties.

This work is the first step in the understanding of the complex behavior of hydrogen insertion in transition metal doped V systems. It would be also of prime importance to understand how the doping affects the H-H interaction by considering the loading with higher hydrogen concentrations. Work in this line is currently undertaken.

ACKNOWLEDGMENTS

We acknowledge the financial support from the Spanish Ministry of Science and Innovation in conjunction with the European Regional Development Fund (Project No. FIS2008-02490/FIS) and the Junta de Castilla y León (Project No. GR120). A.V. acknowledges the financial support and the kind hospitality from the Université de Brest (UBO), France. The authors acknowledge the numerical support of the Pole de Calcul Intensif pour la Mer (Brest) and the Pole de Calcul Intensif des Pays de la Loire (Nantes).

*Permanent address: Departamento de Física Teórica, Atómica y Óptica, Universidad de Valladolid, Spain.

[1] P. Vajeeston, P. Ravindran, and H. Fjellvag, J. Alloys Compd. **446-447**, 44 (2007).
[2] Y. Filinchuk, D. Chernyshov, A. Nevidomskyy, and V. Dmitriev, Angew. Chem., Int. Ed. **47**, 529 (2008).
[3] Y. Filinchuk, R. Czerny, and H. Hagemann, Chem. Mater. **21**, 925 (2009).
[4] M. Gupta and R. P. Gupta, J. Alloys Compd. **446-447**, 319 (2007).
[5] L.-P. Ma, P. Wang, H.-B. Dai, L.-Y. Kong, and H.-M. Cheng, J. Alloys Compd. **466**, L1 (2008).
[6] H. Arashima, F. Takahashi, T. Ebisawa, H. Itoh, and T. Kabutomori, J. Alloys Compd. **356-357**, 405 (2003).
[7] T. Huang, Z. Wu, G. Sun, and N. Xu, J. Alloys Compd. **450**, 505 (2008).
[8] K. Kobayashi, M. Yamauchi, H. Kitagawa, Y. Kubota, K. Kato, and M. Takata, J. Am. Chem. Soc. **130**, 1818 (2008).
[9] B. Skubic, E. Holmstrőm, A. Bergman, and O. Eriksson, Phys. Rev. B **77**, 144408 (2008).
[10] S. Ostanin, V. M. Uzdin, C. Demangeat, J. M. Wills, M. Alouani, and H. Dreyssé, Phys. Rev. B **61**, 4870 (2000).
[11] V. Leiner, K. Westerholt, A. M. Blixt, H. Zabel, and B. Hjőrvarsson, Phys. Rev. Lett. **91**, 037202 (2003).
[12] D. Labergerie, K. Westerholt, H. Zabel, and B. Hjőrvarsson, J. Magn. Magn. Mater. **225**, 373 (2001).
[13] A. Remhof, G. Nowak, A. Nefedov, H. Zabel, M. Bjőrck, M. Parnaste, and B. Hjőrvarsson, Superlattices Microstruct. **41**, 127 (2007).
[14] G. Andersson, B. Hjőrvarsson, and H. Zabel, Phys. Rev. B **55**, 15905 (1997).
[15] T. Dziekan, V. Meded, S. Mirbt, S. Shallcross, B. Hjőrvarsson, and P. Zahn, Phys. Rev. B **79**, 012402 (2009).
[16] V. Meded and S. Mirbt, Phys. Rev. B **71**, 024207 (2005).
[17] A. K. Eriksson, A. Liebig, S. Olafsson, and B. Hjőrvarsson, J. Alloys Compd. **446-447**, 526 (2007).
[18] V. Meded, S. Olsson, P. Zahn, B. Hjőrvarsson, and S. Mirbt, Phys. Rev. B **69**, 205409 (2004).
[19] A. Lebon, A. Mokrani, and A. Vega, Phys. Rev. B **78**, 184401 (2008).
[20] http://www.webelements.com and B. Cordero, V. Gomez, A. E. Platero-Prats, M. Reves, J. Echeverria, E. Cremades, F. Baregan, and S. Alvarez, Dalton Trans. **21**, 2832 (2008).
[21] J. M. Soler, E. Artacho, J. D. Gale., A. García, J. Junquera, P. Ordejon, and D. Sánchez-Portal, J. Phys.: Condens. Matter **14**, 2745 (2002).
[22] P. Ordejon, E. Artacho, and J. M. Soler, Phys. Rev. B **53**, R10441 (1996).
[23] D. Sanchez-Portal, P. Ordejon, E. Artacho, and J. M. Soler, Int. J. Quantum Chem. **65**, 453 (1997).
[24] J. P. Perdew, K. Burke, and M. Ernzerhof, Phys. Rev. Lett. **77**, 3865 (1996).
[25] S. G. Louie, S. Froyen, and M. L. Cohen, Phys. Rev. B **26**, 1738 (1982).
[26] N. Troullier and J. L. Martins, Phys. Rev. B **43**, 1993 (1991).
[27] L. Kleinman and D. M. Bylander, Phys. Rev. Lett. **48**, 1425 (1982).
[28] M. B. Torres, E. M. Fernandez, and L. C. Balbas, Phys. Rev. B **75**, 205425 (2007).
[29] R. C. Longo, M. M. G. Alemany, A. Vega, J. Ferrer, and L. J. Gallego, Nanotechnology **19**, 245701 (2008).
[30] E. M. Fernandez, M. B. Torres, and L. C. Balbas, Int. J. Quantum Chem. **99**, 39 (2004).
[31] R. Robles, J. Izquierdo, A. Vega, and L. C. Balbas, Phys. Rev. B

63, 172406 (2001).
[32] G. Kresse and D. Joubert, Phys. Rev. B **59**, 1758 (1999).
[33] J. Izquierdo, A. Vega, L. C. Balbas, D. Sanchez-Portal, J. Junquera, E. Artacho, J. M. Soler, and P. Ordejon, Phys. Rev. B **61**, 13639 (2000).
[34] F. Tournus and J.-C. Charlier, Phys. Rev. B **71**, 165421 (2005).
[35] K. Lee, J. Yu, and Y. Morikawa, Phys. Rev. B **75**, 045402 (2007).
[36] G. Andersson, B. Hjőrvarsson, and P. Isberg, Phys. Rev. B **55**, 1774 (1997).
[37] L. C. Duda, P. Isberg, P. H. Andersson, P. Skytt, B. Hjőrvarsson, J. H. Guo, C. Sathe, and J. Nordgren, Phys. Rev. B **55**, 12914 (1997).
[38] J. Bloch, B. Hjőrvarsson, S. Olsson, and R. Brukas, Phys. Rev. B **75**, 165418 (2007).